Eur Radiol (2006) 16: 1709–1718
DOI 10.1007/s00330-006-0166-9

Hiromichi Fukushima
Shigeki Itoh
Akira Takada
Yoshimi Mori
Kojiro Suzuki
Akiko Sawaki
Shingo Iwano
Hiroko Satake
Toyohiro Ota
Mitsuru Ikeda
Takeo Ishigaki

Diagnostic value of curved multiplanar reformatted images in multislice CT for the detection of resectable pancreatic ductal adenocarcinoma

Received: 15 August 2005
Revised: 29 October 2005
Accepted: 17 January 2006
Published online: 21 March 2006

H. Fukushima (✉) · A. Takada · Y. Mori · K. Suzuki · A. Sawaki · S. Iwano · H. Satake · T. Ota · T. Ishigaki
Department of Radiology,
Nagoya University School of Medicine,
65 Tsurumai-cho, Showa-ku,
Nagoya 466-8560, Japan
e-mail: suncus@yahoo.co.jp
Tel.: +81-52-7442327
Fax: +81-52-7442335

S. Itoh · M. Ikeda
Department of Technical Radiology,
Nagoya University School of Health Sciences,
Nagoya, Japan

Abstract The purpose of this study was to assess the usefulness of curved multiplanar reformatted (MPR) images obtained by multislice CT for the depiction of the main pancreatic duct (MPD) and detection of resectable pancreatic ductal adenocarcinoma. This study included 28 patients with pancreatic carcinoma (size range 12–40 mm) and 22 without. Curved MPR images with 0.5-mm continuous slices were generated along the long axis of the pancreas from pancreatic-phase images with a 0.5- or 1-mm slice thickness. Seven blinded readers independently interpreted three sets of images (axial images, curved MPR images, and both axial and curved MPR images) in scrolling mode. The depiction of the MPD and the diagnostic performance for the detection of carcinoma were statistically compared among these images. MPR images were significantly superior to axial images in depicting the MPD, and the use of both axial and MPR images resulted in further significant improvements. For the detection of carcinoma, MPR images were equivalent to axial images, and the diagnostic performance was significantly improved by the use of both axial and MPR images. High-resolution curved MPR images can improve the depiction of the MPD and the diagnostic performance for the detection of carcinoma compared with axial images alone.

Keywords Pancreas · Pancreatic ductal adenocarcinoma · Multislice CT · Multiplanar reformatted image

Abbreviations cMPR: curved multiplanar reformatted

Introduction

During the past few years, the incidence of pancreatic ductal adenocarcinoma has increased in almost all parts of the world [1]. Although surgical resection is the only potentially curative therapy, only 5–30% of patients with pancreatic carcinoma are considered candidates for resection at the initial diagnosis, and the prognosis for most patients is extremely poor, with an overall 5-year survival rate of less than 5% [2, 3]. However, patients with tumors 20–30 mm or less had 5-year survival rates of 33–38% [4–6]. Therefore, the detection of small tumors at the earliest possible stage is crucial in improving the outcome of patients with this carcinoma.

Since patients with pancreatic carcinoma do not present with clinically relevant signs or symptoms before the disease reaches an advanced stage, diagnostic imaging plays an important role in detection. Computed tomography (CT) is the most commonly employed imaging modality for the evaluation of known or suspected diseases of the pancreas, and it is important to avoid missing small and potentially resectable carcinomas in such examinations. Although previous studies using single-slice CT have reported that contrast-enhanced helical CT has a sensitivity of 89–97% for tumor detection, this high sensitivity is in part due to the advanced stage of many tumors [7–10]. In previous studies, the sensitivity for the detection of pancreatic masses measuring 20 mm or less was reported

to be only 58–77%, even with the use of multislice CT [11–13].

Multislice CT, with its faster Z-axis speeds, makes it possible to scan the pancreas and biliary system with a collimation of 1.25 mm or less during a single breath-hold. This results in further improvements in the quality of multiplanar reformatted (MPR) images due to the superior resolution in the Z-axis. It has recently been reported that the use of such high-quality MPR images provides more accurate information concerning the vascular invasion and resectability of pancreatic carcinoma [9, 14–17]. However, to our knowledge, the capabilities of curved MPR images for the detection of this carcinoma have been evaluated in only a single report [8]. The present study was therefore conducted to assess the usefulness of MPR images generated from 1-mm-thick or 0.5-mm-thick images obtained by multislice CT for depicting the main pancreatic duct and detecting resectable pancreatic ductal adenocarcinomas as compared to axial images alone.

Materials and methods

Patients

The surgical records of the patients treated at our institution from May 2000 to April 2003 were retrospectively reviewed, and 28 consecutive patients (15 men and 13 women; age range 33–83 years; mean age 62.1 years) with pancreatic ductal adenocarcinoma were identified based on the following inclusion criteria: (1) appropriate CT examinations were performed in accordance with our protocol, (2) the tumor was surgically resected, (3) the diagnosis was histopathologically confirmed, and (4) the diameter of the tumor was 40 mm or less in the resected specimens. The mean diameter of the carcinomas was 27 mm (range 12–40 mm) in the resected specimens, and 23 of the 28 tumors (82.1%) were 30 mm or less in diameter (Table 1).

Table 1 Patients with pancreatic ductal adenocarcinoma

Sex (male/female)		15/13
Age (years)	Mean	62.1
	Range	33–83
Location of the lesion	Head	18*
	Neck	7*
	Body	4
	Tail	0
Diameter of the lesion	≤2 cm	11
	>2 cm, ≤3 cm	12
	>3 cm, ≤4 cm	5

*One lesion extended from pancreatic head to neck

As the control group, 22 consecutive patients (12 men and 10 women; age range 24–70 years; mean age 53.1 years) were selected based on the following inclusion criteria: (1) appropriate CT studies were performed for the evaluation of suspected pancreatic tumors in accordance with the same protocol and during the same period and (2) the absence of pancreatic tumors was confirmed based on the clinical course and a combination of various imaging findings, with follow-up for at least 18 months (mean 29 months; range 18–42 months). The final diagnoses were chronic pancreatitis (12 patients), autoimmune pancreatitis (1 patient), acute pancreatitis (1 patient), and no significant abnormality (8 patients).

The CT examination in this study was conducted in accordance with the established clinical standards of our institution, and each patient agreed to undergo the examinations after the purpose, methods, and risk of the CT examination had been fully explained. Our institutional review board approved the retrospective data collection and analysis for this research, with informed consent from the patients waived.

CT image acquisition

CT scanning was performed using a multislice CT scanner with four detector rows (Aquilion, Toshiba, Tokyo, Japan). Five minutes before scanning, the patient was instructed to drink 300 ml of water for negative opacification of the gastrointestinal tract. Nonionic contrast material with an iodine concentration of 300 mgI/ml was injected at 0.08 ml/kg body weight/s over 30 s, and a 5% dextrose flush was administered at a fixed rate of 5 ml/s over 6 s immediately after the end of contrast material injection. The injection of both contrast material and 5% dextrose was performed using two automatic power injectors (Auto enhance A50, Auto injector 1205, Nemotokyorindo, Tokyo) via a 20-gauge intravenous catheter placed in an antecubital vein.

First, unenhanced images were acquired in order to determine the range in the Z-axis of the liver and pancreas in all patients. In the 12 patients who underwent three-phase contrast-enhanced CT studies, arterial-phase and pancreatic-phase scanning from the porta hepatis to the end of the duodenum were performed with a detector row configuration of 4×1 mm and a table increment of 5.5 mm/rotation during a single breath-hold (Table 2). For the patients who were more than 60 years old and/or had cardiovascular disease, arterial-phase scanning was started as soon as possible (9 s on average) after the attenuation value in the aorta (at the same level as the start position of scanning) reached a value of 80 HU or higher using the automatic bolus-tracking method (SureStart, Toshiba, Tokyo). For the other patients, the scan delay from the administration of contrast material to the start of arterial-phase scanning was set at 24 s.

Table 2 Scan parameters for three-phase contrast-enhanced CT

Parameter	Pre-enhancement	Enhanced	
		Arterial Pancreatic	Portal
Target structures	Liver, Pancreas	Biliary tract, Pancreas	Liver, Pancreas
Direction	Cephalocaudal	*1	Cephalocaudal
Tube voltage	120 kVp	120 kVp	120 kVp
Tube current	300 mA	300 mA	300 mA
Gantry rotation speed	0.5 s	0.5 s	0.5 s
Detector row configuration	4×3 mm	4×1 mm	4×1 mm
Table increment*2	9	5.5	5.5
Helical pitch*3	0.75	1.375	1.375
Weighted CT dose index	18.6 mGy	16.2 mGy×2	16.2 mGy

*1: Two sequential acquisitions (with an inter-scan delay of 5 s) are performed during a single breath-hold in the cephalocaudal direction for the arterial phase and in the caudocephalad direction for the pancreatic phase; *2: mm/360°gantry rotation; *3: table increment/overall width of active detectors

In the 38 patients who underwent dual-phase contrast-enhanced CT studies, pancreatic-phase scanning from the porta hepatis to the end of the duodenum was performed with a detector row configuration of 4×0.5 mm and a table increment of 2.75 mm/rotation (Table 3). For the patients who were more than 60 years old and/or had cardiovascular disease, pancreatic-phase scanning was started at 11 s after the attenuation value in the aorta reached a value of 130 HU or higher using the automatic bolus-tracking method. For the other patients, the scan delay from the administration of contrast material to the start of pancreatic-phase scanning was set at 30 s.

In both protocols, the pancreas in pancreatic-phase images was scanned during the period 40–50 s on average from the administration of contrast material in order to achieve intense contrast enhancement of the pancreatic parenchyma based on the results of previous studies [18, 19]. Other scan parameters were the same in both protocols, and the time interval between the pancreatic and portal phases was fixed at 15 s.

Image processing and interpretation

In the present study, the pancreatic-phase images were reconstructed with a 0.5-mm slice thickness at 0.5-mm intervals or a 1-mm slice thickness at 0.5-mm intervals over a 260-mm field of view. The images were transferred to a workstation (Aquarius Workstation, ELK Corporation, Osaka). One radiologist generated the curved MPR images with a 0.5-mm slice thickness at 0.5-mm intervals to cover the pancreatic parenchyma. In order to generate the curved MPR images, the operator designated a curved line along the long axis of the pancreas by scrolling and reviewing a stack of axial images, and multiple images were generated parallel to this curved plane (Fig. 1).

Seven experienced radiologists who were blinded to other imaging findings and the diagnosis interpreted the images in scrolling mode. Each observer assessed three sets of images (0.5-mm or 1-mm axial images alone, curved MPR images alone, and both axial and curved MPR images) independently at intervals of at least 2 weeks. The reading order was balanced so that four observers

Table 3 Scan parameters for dual-phase contrast-enhanced CT

Parameter	Pre-enhancement	Enhanced	
		Pancreatic	Portal
Target structures	Liver, Pancreas	Biliary tract, Pancreas	Liver, Pancreas
Direction	Cephalocaudal	Cephalocaudal	Cephalocaudal
Tube voltage	120 kVp	120 kVp	120 kVp
Tube current	300 mA	300 mA	300 mA
Gantry rotation speed	0.5 s	0.5 s	0.5 s
Detector row configuration	4×3 mm	4×0.5 mm	4×1 mm
Table increment*1	9	2.75	5.5
Helical pitch*2	0.75	1.375	1.375
Weighted CT dose index	18.6 mGy	24.1 mGy	16.2 mGy

*1: mm/360°gantry rotation; *2: table increment/overall width of active detectors

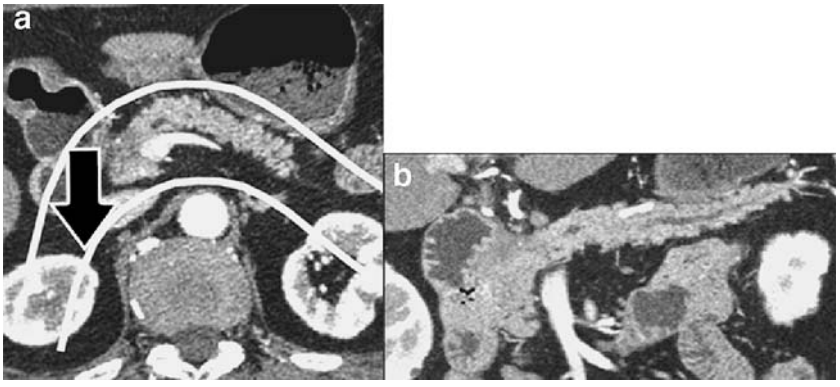

Fig. 1 Generation of curved multiplanar reformatted images. The curved planes for multiplanar reformatted images are selected to follow the long axis of the pancreas (**a**). Curved multiplanar reformatted images (**b**) are reconstructed with 0.5-mm thickness at 0.5-mm intervals to cover the pancreas. *Arrow* indicates the order of presentation of the images

interpreted the axial images before the MPR images, and the other three interpreted the MPR images before the axial images. In addition, all observers interpreted both the axial and MPR images. Finally, the reading order for patient images also differed among the seven observers.

The pancreas of each patient was divided into four segments: the head, neck, body, and tail. The neck was defined as the segment ventral to the confluence of the superior mesenteric vein and splenic vein. The portion upstream from the neck was divided into two equal segments: the body and the tail. Each observer reported the following items for each segment of each patient: (1) the degree of depiction of the main pancreatic duct (using a continuous rating scale from 0 to 100%) and (2) the confidence level for the presence of pancreatic ductal adenocarcinoma (using a continuous rating scale from 0 to 1, with values of 0 and 1 corresponding to the definite absence and the definite presence of pancreatic ductal adenocarcinoma, respectively). The observers were not asked to perform an evaluation for vascular invasion or hepatic, nodular, or peritoneal metastasis.

Statistical analysis

With regard to the findings for the main pancreatic duct, two radiologists with knowledge of the diagnosis, basing their judgments on consensus, interpreted all CT images and classified each duct in each segment as follows: (1) 2 mm or less, greater than 2 mm up to 4 mm, or greater than 4 mm in diameter and (2) the presence or absence of stenosis or occlusion of the upper stream. The diameter was measured at the workstation with electronic calipers. Twenty-five segments were excluded from further analysis because it was judged that the presence of carcinomas (n=23) or drainage tubes (n=2) interfered with the evaluation for the depiction of the main pancreatic duct.

We determined the sensitivity, specificity, accuracy, positive predictive value, and negative predictive value for the detection of pancreatic ductal adenocarcinoma. In this analysis, when the confidence level for the presence of carcinoma was reported to be 50% or more at least in one segment, the judgment for the patient was accepted as positive. Furthermore, each reader's judgment regarding the presence or absence of pancreatic ductal carcinoma was assessed using the Brier score [20, 21], which is calculated by the following equation:

$$B = \frac{1}{n}\sum_{i=1}^{n}(Pi - Ti)^2$$

where n is the total number of segments, Pi is the confidence level for the presence of pancreatic ductal carcinoma in each segment, and Ti is 1 if a carcinoma is present and 0 if a carcinoma is absent. The lower this score, the more certain the reader's judgment was concerning the presence or absence of pancreatic ductal carcinoma.

All interpretations of the seven observers underwent collective statistical analysis to determine whether there were any significant differences among the three sets of images (0.5 or 1-mm axial images, curved MPR images, and both axial and curved MPR images) for the depiction of the main pancreatic duct and the detection of pancreatic ductal carcinoma. Statistical analysis of differences in the depiction of the main pancreatic duct among the three types of interpreted images was performed using analysis of variance (ANOVA) with the type of interpreted images as the fixed effect and the images and the observers as the random effects. Furthermore, in order to evaluate differences in the diagnostic performance for determining the presence of pancreatic carcinoma among the three types of interpreted images, ANOVA of the pseudovalues of Brier scores computed by the jackknife-analysis method was also performed, with the type of interpreted images as the fixed effect and the images and the observers as the random effects. The results of the interpretations were also analyzed for each item (size, location, characteristics, and reader). A value of P<0.05 was considered statistically significant.

Results

The measurement results for the maximum diameter of the main pancreatic duct were 2 mm or less for 61 segments (34.8%), greater than 2 mm up to 4 mm for 64 segments (36.6%), and greater than 4 mm for 50 segments (28.6%). It was judged that the main pancreatic duct was free of stenosis or obstruction upstream in 103 of 175 segments (58.9%).

With regard to the depiction of the main pancreatic duct, the results for curved MPR images alone were significantly superior to those for axial images alone, and the use of both axial and curved MPR images resulted in further significant improvements. The use of curved MPR images helped to improve the depiction of the duct, especially in the following situations: (1) duct located in the pancreatic head and neck, (2) duct diameter less than 4 mm, and (3) no stenosis or obstruction upstream (Table 4, Fig. 2).

With regard to the detection of pancreatic ductal adenocarcinoma, the sensitivity, specificity, accuracy, positive predictive value, and negative predictive value of axial images alone, curved MPR images alone, and both axial and curved MPR images were 78.6, 91.6, 84.2, 92.2, and 77.0%, and 75.5, 91.6, 82.6, 91.9, and 74.6%, and 90.8, 94.2, 92.3, 95.2, and 89.0%, in the collective results, respectively (Table 5). In the assessment using the Brier score, the results for curved MPR images alone were equivalent to those for axial images alone, and the use of both axial and curved MPR images made it possible to improve the diagnostic performance for determining the presence or absence of carcinoma significantly as compared with either axial images alone or curved MPR images alone. The same trend was observed in the results for each reader. In particular, the use of both axial and curved MPR images helped to determine the presence or absence of carcinoma, especially in the following situations: (1) tumor located in the pancreatic head and neck and (2) tumor diameter 30 mm or less (Table 6, Figs. 3, 4).

Discussion

Curved MPR images allow single two-dimensional image display of structures that run through multiple oblique planes. Software that is capable of automatically extracting the median centerline of vessels and creating curved planar reformations has been developed [8]. However, since this method has not yet been optimized for the pancreatic duct, in order to evaluate the duct using single-slice curved MPR images accurately, the operator is required to place a cursor on a stack of axial, sagittal, or coronal sections exactly along the course of the center of the duct. This procedure requires a high degree of skill and is often troublesome in cases without dilatation of the pancreatic ducts. Furthermore, tumors are not necessarily visualized most conspicuously in the curved plane along the course of the center of the duct. Therefore, in the present study, we employed a protocol in which curved MPR images were generated with a 0.5-mm slice thickness at 0.5-mm intervals to cover the pancreatic parenchyma, and these images were reviewed in scrolling mode.

Pancreatic carcinomas generally appear as hypoattenuated areas compared with surrounding pancreatic parenchyma in contrast-enhanced CT [7, 22]. However, previous studies have reported that some tumors show isoattenuation compared with the surrounding pancreatic parenchyma in pancreatic-phase scans or in both pancreatic-phase and portal-phase scans and that the following ancillary signs should be carefully evaluated in order to avoid missing such tumors: (1) a focal change in texture at the tumor, (2)

Table 4 Results for depiction of main pancreatic duct

Image		Axial (%)	cMPR* (%)	Axial+cMPR (%)
Total		75.1 (70.8–79.4)	84.2† (79.8–88.6)	86.9†# (82.3–91.5)
Location	Head (*n*=35)	60.6 (51.6–70.0)	80.0† (72.4–87.6)	79.9† (72.0–87.8)
	Neck (*n*=42)	77.8 (69.7–86.0)	89.1† (83.2–95.0)	90.5† (85.1–95.9)
	Body (*n*=48)	86.9 (81.0–92.8)	90.6† (85.5–95.6)	93.2† (88.6–97.9)
	Tail (*n*=50)	71.7 (63.2–80.1)	76.9† (67.8–86.0)	82.7†# (74.0–91.4)
Diameter of the main pancreatic duct	≤2 mm (*n*=74)	63.5 (55.6–71.5)	74.8† (67.5–82.2)	79.2†# (70.7–87.7)
	>2 mm, ≤4 mm (*n*=51)	73.3 (66.8–79.8)	85.3† (79.9–90.8)	86.5† (81.4–91.5)
	>4 mm (*n*=50)	91.7 (88.4–94.9)	94.2† (91.0–97.4)	96.9†# (95.1–98.7)
Stenosis or obstruction of the upstream	(+) (*n*=72)	88.2 (84.3–92.1)	91.1† (86.6–95.6)	94.5†# (91.3–97.7)
	(−) (*n*=103)	66.0 (60.2–71.8)	79.4† (74.0–84.8)	81.6† (75.6–87.7)

Figures in parentheses indicate 95% confidence intervals. The diameter is measured at the workstation with electronic calipers. * Curved multiplanar reformatted; † significantly superior to axial images alone by analysis of variance (P<0.05); # significantly superior to curved MPR images alone by analysis of variance (P<0.05)

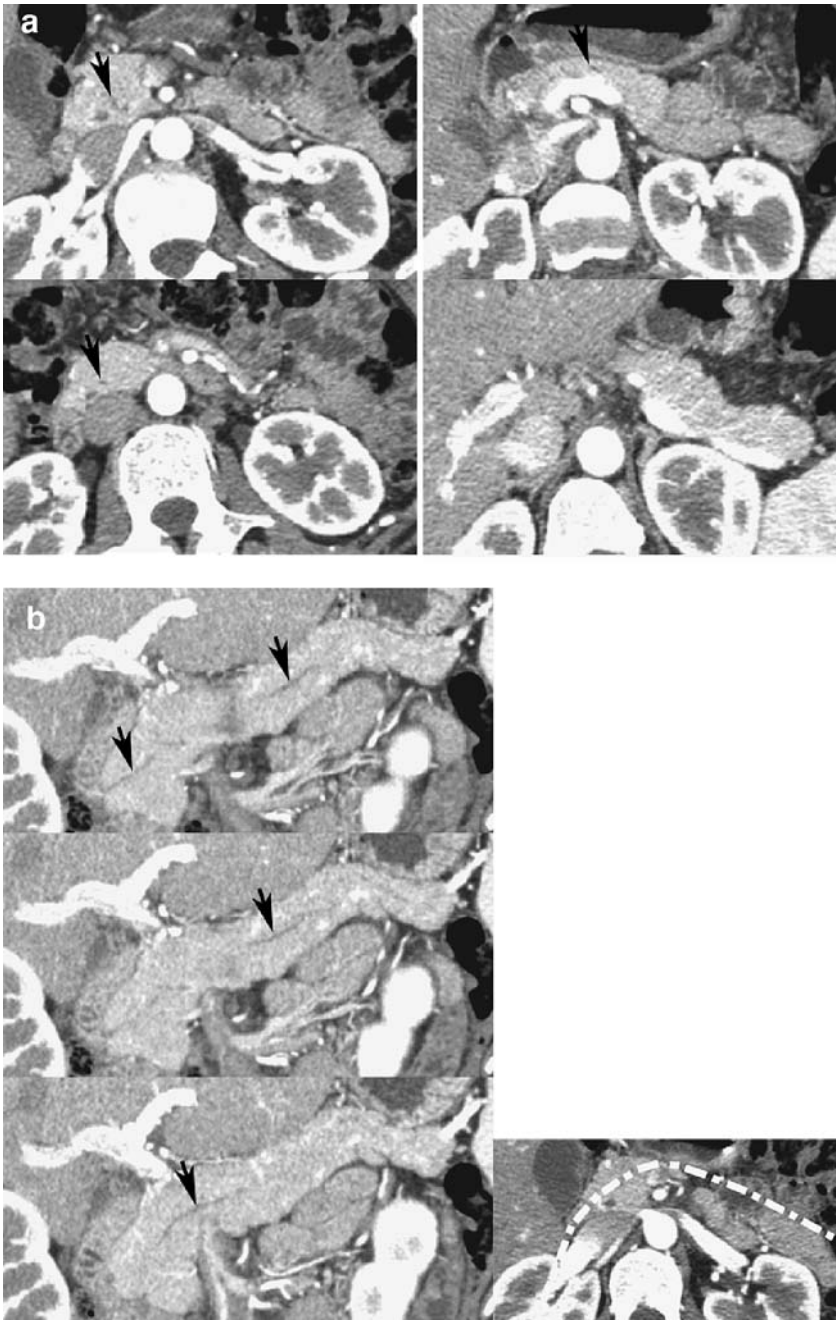

Fig. 2 Main pancreatic duct in the axial and curved multiplanar reformatted images (41-year-old female). The main pancreatic duct (*arrows*) is more clearly and more continuously demonstrated in curved multiplanar reformatted images (**b**) than in axial images (**a**). Furthermore, the use of both axial and curved multiplanar reformatted images makes it possible to confirm more confidently that the entire pancreatic parenchyma shows homogenous enhancement without contour deformity

dilatation of the main pancreatic duct upstream from the tumor, (3) atrophy of the pancreatic parenchyma upstream from the tumor, (4) a clear convex contour deformity of the pancreatic parenchyma at the level of the tumor, and (5) delayed enhancement of the tumor [10, 23, 24]. However, there is notable interobserver variation in the perception and analysis of the visualization of textural changes. Among the remaining findings, dilatation of the main pancreatic duct upstream from the tumor (the so-called interrupted duct sign) is most frequently observed [10, 23, 24], and this is also an important clue for distinguishing between pancreatic carcinoma and chronic pancreatitis [25].

The results of the present study have demonstrated that curved MPR images obtained by multislice CT are significantly superior to axial images in the depiction of the main pancreatic duct. These results are in agreement with those of previous studies using oblique MPR images [26, 27]. These findings indicate that the MPR images generated from isotropic or nearly isotropic volumetric data sets provide sufficient resolution in the Z-axis for accurate evaluation of the main pancreatic duct and are more

Table 5 Results for detection of pancreatic ductal adenocarcinoma

	Axial			cMPR*			Axial+cMPR		
	Sensitivity	Specificity	Accuracy	Sensitivity	Specificity	Accuracy	Sensitivity	Specificity	Accuracy
Total	154/196 (78.6)	141/154 (91.6)	295/350 (84.2)	148/196 (75.5)	141/154 (91.6)	289/350 (82.6)	178/196 (90.8)	145/154 (94.2)	323/350 (92.3)
Reader 1	25/28 (89.3)	18/22 (81.8)	43/50 (86.0)	22/28 (78.6)	20/22 (90.9)	42/50 (84.0)	25/28 (89.3)	20/22 (90.9)	45/50 (90.0)
Reader 2	21/28 (75.0)	21/22 (95.5)	42/50 (84.0)	21/28 (75.0)	20/22 (90.9)	41/50 (82.0)	24/28 (85.7)	21/22 (95.5)	45/50 (90.0)
Reader 3	21/28 (75.0)	21/22 (95.5)	42/50 (84.0)	23/28 (78.6)	20/22 (90.9)	43/50 (86.0)	27/28 (96.4)	21/22 (95.5)	48/50 (96.0)
Reader 4	23/28 (82.1)	20/22 (90.9)	43/50 (86.0)	23/28 (82.1)	22/22 (100)	45/50 (90.0)	26/28 (92.9)	22/22 (100)	48/50 (96.0)
Reader 5	19/28 (67.9)	22/22 (100)	41/50 (82.0)	20/28 (71.4)	18/22 (81.8)	38/50 (76.0)	26/28 (92.9)	20/22 (90.9)	46/50 (92.0)
Reader 6	22/28 (78.6)	19/22 (86.4)	41/50 (82.0)	19/28 (67.9)	21/22 (95.5)	40/50 (80.0)	23/28 (82.1)	21/22 (95.5)	44/50 (88.0)
Reader 7	23/28 (82.1)	20/22 (90.9)	43/50 (86.0)	20/28 (71.4)	20/22 (90.9)	40/50 (80.0)	27/28 (96.4)	20/22 (90.9)	47/50 (94.0)

When the confidence level for the presence of carcinoma was reported to be 50% or more at least in one segment, the judgment for the patient is accepted as positive. Numbers in parentheses are percentages. * Curved multiplanar reformatted

suitable for following the course of the duct than axial images. This advantage of high-resolution MPR images makes it possible to detect partial obstruction of the pancreatic duct by a tumor with greater certainty, which may be helpful for the detection of pancreatic carcinoma showing isoattenuation compared with the surrounding pancreatic parenchyma.

In the present study as well as the study of Prokesch et al. [8], curved MPR images were found to be equivalent to axial images for the detection of pancreatic ductal adenocarcinoma. However, it has been demonstrated that the diagnostic performance for determining the presence or absence of carcinoma can be significantly improved by using both axial and curved MPR images, and this improvement is particularly noticeable for tumors measuring 30 mm or less in diameter and tumors located in the pancreatic head and neck. Due to the complex anatomy of the pancreaticobiliary region, axial images are not necessarily optimal for visualizing changes in the contours and contrast-enhancement of the pancreatic parenchyma as well as the spatial relationships of pancreatic tumors with surrounding structures. From the results of this study, it is concluded that, compared with axial images alone, the use of curved MPR images provides additional information

Table 6 Brier score: results for detection of pancreatic ductal adenocarcinoma

Image		Axial	cMPR*	Axial+cMPR
Total		0.0431 (0.0237–0.0625)	0.0390 (0.0219–0.0561)	0.0208†# (0.0101–0.0315)
Reader 1		0.0426	0.0333	0.0257
Reader 2		0.0408	0.0428	0.0264
Reader 3		0.0452	0.0330	0.0097
Reader 4		0.0489	0.0375	0.0225
Reader 5		0.0452	0.0452	0.0203
Reader 6		0.0432	0.0399	0.0239
Reader 7		0.0356	0.0411	0.0169
Location	Head	0.1094 (0.0500–0.1688)	0.1050 (0.0503–0.1597)	0.0528†# (0.0166–0.0890)
	Neck	0.0556 (0.0081–0.1031)	0.0450 (0.0066–0.0834)	0.0261† (0.0060–0.0462)
	Body	0.0057 (0.0000–0.0126)	0.0043 (0.0002–0.0084)	0.0025 (0.0000–0.0055)
Diameter of the tumor	≤20 mm	0.0303 (0.0120–0.0486)	0.0262 (0.0115–0.0409)	0.0164†# (0.0065–0.0263)
	>20 mm, ≤30 mm	0.0225 (0.0099–0.0351)	0.0206 (0.0080–0.0332)	0.0110†# (0.0047–0.0173)
	>30 mm, ≤40 mm	0.0104 (0.0047–0.0161)	0.0088 (0.0040–0.0136)	0.0058† (0.0022-0.0094)

The lower the Brier score, the more certain the reader's judgment was concerning the presence of pancreatic ductal adenocarcinoma. Figures in parentheses indicate 95% confidence intervals. *Curved multiplanar reformatted; † significantly superior to axial images alone by analysis of variance ($P<0.05$); # significantly superior to curved MPR images alone by analysis of variance ($P<0.05$)

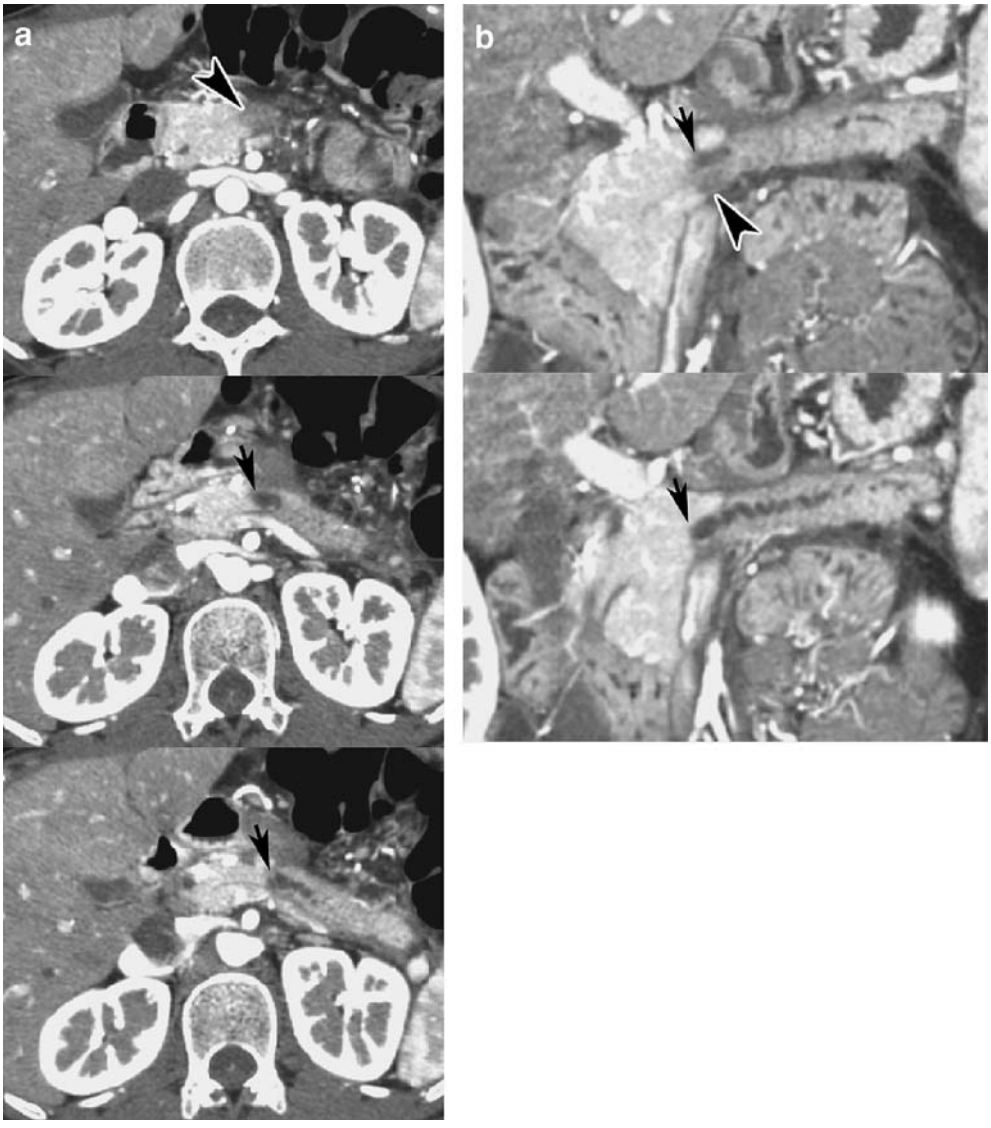

Fig. 3 Pancreatic ductal adenocarcinoma (46-year-old male). The focal hypoattenuated area (*arrowhead*) with the diameter of 15 mm is observed in the neck of the pancreas. The upstream main pancreatic duct (*arrows*) shows moderate dilatation. In comparison with axial images alone (**a**), the combined use of curved multiplanar reformatted images (**b**) makes it possible to confirm the presence of carcinoma with greater certainty by visualizing the spatial relationship of the hypoattenuated area with the dilated main pancreatic duct more clearly

concerning these points and improves the observer's confidence in determining the presence or absence of carcinoma (Figs. 3, 4). Although it takes approximate 2–3 min to generate and interpret the curved MPR images as described in this study, in order to avoid missing small and resectable carcinomas, we recommend the combined use of such images in cases in which the presence of a pancreatic tumor is clinically suspected.

The present study suffers from a number of limitations. One possible bias involves the degree of familiarity that the observers had with each type of image. Specifically, the observers had substantially less experience in reviewing curved MPR images as compared with axial images. In the present study, all observers interpreted both the axial and MPR images after the axial images alone and the curved MPR images alone. This may have introduced additional memory bias, which could have skewed the interpretation of the images. In addition, the number of patients was relatively small, and this study included only 11 tumors measuring 20 mm or less in diameter, for which patients might be expected to have a less unsatisfactory outcome than those with unresectable tumors. In order to overcome the limitations in statistical power, we employed a protocol in which the number of observers was seven. However, it would be desirable to carry out further studies in large populations in order to determine the most suitable clinical applications of curved MPR images in detecting pancreatic ductal adenocarcinomas measuring 20 mm or less in diameter.

It has recently been reported that oblique MPR images following the course of the main pancreatic duct are useful for evaluating the region of the pancreatic head [28, 29]. Compared with curved MPR images used in the present study, oblique MPR images may be generated more easily, but the selection of the appropriate oblique angle is required for each location of the pancreas. On the other hand, in

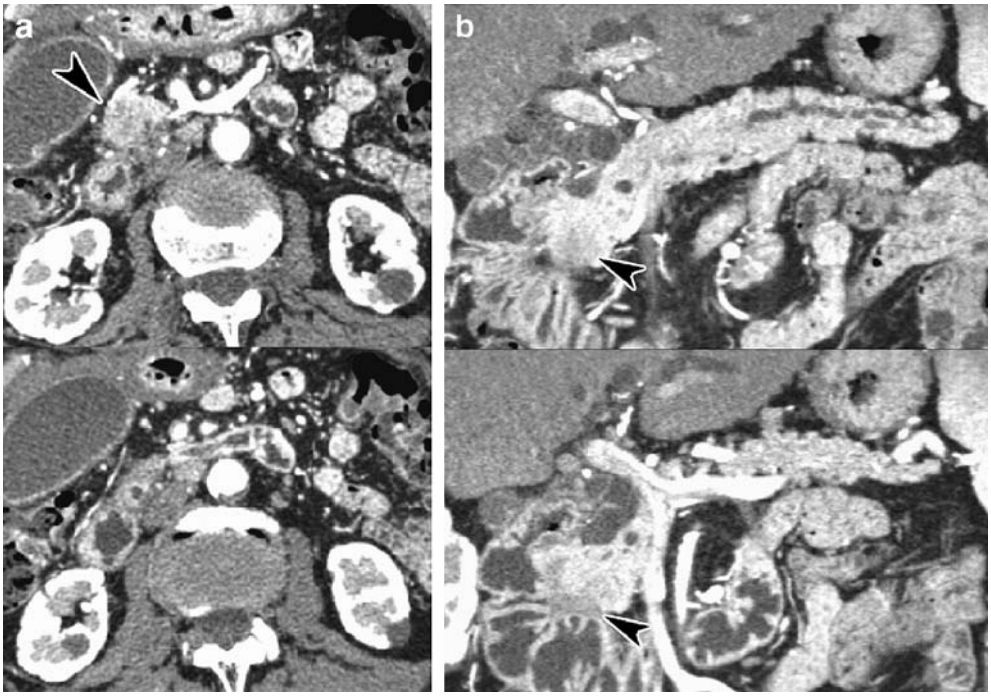

Fig. 4 Pancreatic ductal adenocarcinoma (76-year-old male). The focal hypoattenuated area (*arrowhead*) with the diameter of 30 mm is observed in the head of the pancreas. The upstream main pancreatic duct shows moderate dilatation. In comparison with axial images alone (**a**), the combined use of curved multiplanar reformatted images (**b**) makes it possible to confirm the presence of carcinoma with greater certainty by visualizing the spatial relationship of the hypoattenuated area with the duodenum more clearly

curved MPR images, the plane along the long axis of the pancreas is always employed regardless of the location of the specific lesion. Further studies should be carried out in order to determine the most suitable clinical applications of these two types of MPR images.

In conclusion, the use of curved MPR images generated from 1-or 0.5-mm-thick images obtained by multislice CT can improve the depiction of the main pancreatic duct and permit the presence or absence of pancreatic ductal adenocarcinoma to be determined with greater certainty as compared with axial images alone.

References

1. Sahmoun AE, D'Agostino RA Jr, Bell RA, Schwenke DC (2003) International variation in pancreatic cancer mortality for the period 1955–1998. Eur J Epidemiol 18:801–816
2. Cooperman AM, Kini S, Snady H, Bruckner H, Chamberlain RS (2000) Current surgical therapy for carcinoma of the pancreas. J Clin Gastroenterol 31:107–113
3. Wray CJ, Ahmad SA, Matthews JB, Lowy AM (2005) Surgery for pancreatic cancer: recent controversies and current practice. Gastroenterology 128:1626–1641
4. Ozaki H, Hiraoka T, Mizumoto R, Matsuno S, Matsumoto Y, Nakayama T, Tsunoda T, Suzuki T, Monden M, Saitoh Y, Yamauchi H, Ogata Y (1999) The prognostic significance of lymph node metastasis and intrapancreatic perineural invasion in pancreatic cancer after curative resection. Surg Today 29:16–22
5. Fortner JG, Klimstra DS, Senie RT, Maclean BJ (1996) Tumor size is the primary prognosticator for pancreatic cancer after regional pancreatectomy. Ann Surg 223:147–153
6. Benassai G, Mastrorilli M, Quarto G, Cappiello A, Giani U, Forestieri P, Mazzeo F (2000) Factors influencing survival after resection for ductal adenocarcinoma of the head of the pancreas. J Surg Oncol 73:212–218
7. Diehl SJ, Lehmann KJ, Sadick M, Lachmann R, Georgi M (1998) Pancreatic cancer: value of dual-phase helical CT in assessing resectability. Radiology 206:373–378

8. Prokesch RW, Chow LC, Beaulieu CF, Nino-Murcia M, Mindelzun RE, Bammer R, Huang J, Jeffrey RB Jr (2002) Local staging of pancreatic carcinoma with multi-detector row CT: use of curved planar reformations initial experience. Radiology 225: 759–765
9. Catalano C, Laghi A, Fraioli F, Pediconi F, Napoli A, Danti M, Reitano I, Passariello R (2003) Pancreatic carcinoma: the role of high-resolution multislice spiral CT in the diagnosis and assessment of resectability. Eur Radiol 13:149–156
10. Bluemke DA, Cameron JL, Hruban RH, Pitt HA, Siegelman SS, Soyer P, Fishman EK (1995) Potentially resectable pancreatic adenocarcinoma: spiral CT assessment with surgical and pathologic correlation. Radiology 197:381–385
11. Bronstein YL, Loyer EM, Kaur H, Choi H, David C, DuBrow RA, Broemeling LD, Cleary KR, Charnsangavej C (2004) Detection of small pancreatic tumors with multiphasic helical CT. Am J Roentgenol 182:619–623
12. Legmann P, Vignaux O, Dousset B, Baraza AJ, Palazzo L, Dumontier I, Coste J, Louvel A, Roseau G, Couturier D, Bonnin A (1998) Pancreatic tumors: comparison of dual-phase helical CT and endoscopic sonography. Am J Roentgenol 170:1315–1322
13. Ichikawa T, Haradome H, Hachiya J, Nitatori T, Ohtomo K, Kinoshita T, Araki T (1997) Pancreatic ductal adenocarcinoma: preoperative assessment with helical CT versus dynamic MR imaging. Radiology 202:655–662
14. Brugel M, Link TM, Rummeny EJ, Lange P, Theisen J, Dobritz M (2004) Assessment of vascular invasion in pancreatic head cancer with multislice spiral CT: value of multiplanar reconstructions. Eur Radiol 14:1188–1195. Epub 2004 Apr 9
15. Vargas R, Nino-Murcia M, Trueblood W, Jeffrey RB Jr (2004) MDCT in pancreatic adenocarcinoma: prediction of vascular invasion and resectability using a multiphasic technique with curved planar reformations. Am J Roentgenol 182:419–425
16. Brugel M, Rummeny EJ, Dobritz M (2004) Vascular invasion in pancreatic cancer: value of multislice helical CT. Abdom Imaging 29:239–245
17. Nino-Murcia M, Jeffrey RB Jr, Beaulieu CF, Li KC, Rubin GD (2001) Multidetector CT of the pancreas and bile duct system: value of curved planar reformations. Am J Roentgenol 176:689–693
18. Tublin ME, Tessler FN, Cheng SL, Peters TL, McGovern PC (1999) Effect of injection rate of contrast medium on pancreatic and hepatic helical CT. Radiology 210:97–101
19. Itoh S, Suzuki K, Iwano S, Satake H, Ota T, Ikeda M, Ishigaki T (2005) Three-phase CT examination of the pancreatobiliary region using multislice CT with 1-mm collimation. Radiat Med 23:283–291
20. Ikeda M, Ishigaki T, Yamauchi K (2002) Relationship between Brier score and area under the binormal ROC curve. Comput Methods Programs Biomed 67:187–194
21. Ikeda M, Itoh S, Ishigaki T, Yamauchi K (2001) Application of resampling techniques to the statistical analysis of the Brier score. Methods Inf Med 40:259–264
22. Lu DS, Vedantham S, Krasny RM, Kadell B, Berger WL, Reber HA (1996) Two-phase helical CT for pancreatic tumors: pancreatic versus hepatic phase enhancement of tumor, pancreas, and vascular structures. Radiology 199:697–701
23. Prokesch RW, Chow LC, Beaulieu CF, Bammer R, Jeffrey RB Jr (2002) Isoattenuating pancreatic adenocarcinoma at multi-detector row CT: secondary signs. Radiology 224:764–768
24. Itoh S, Satake H, Ohta T, Asai H, Endo T, Ishigaki T (2002) Pancreatic ductal adenocarcinoma showing iso-attenuation in early-phase contrast-enhanced CT: comparison with histopathological findings. Radiat Med 20:59–67
25. Ichikawa T, Sou H, Araki T, Arbab AS, Yoshikawa T, Ishigame K, Haradome H, Hachiya J (2001) Duct-penetrating sign at MRCP: usefulness for differentiating inflammatory pancreatic mass from pancreatic carcinomas. Radiology 221:107–116
26. Itoh S, Ikeda M, Ota T, Satake H, Takai K, Ishigaki T (2003) Assessment of the pancreatic and intrapancreatic bile ducts using 0.5-mm collimation and multiplanar reformatted images in multislice CT. Eur Radiol 13:277–285
27. Takada A, Itoh S, Suzuki K, Iwano S, Satake H, Ota T, Ikeda M, Ishigaki T (2005) Branch duct-type intraductal papillary mucinous tumor: diagnostic value of multiplanar reformatted images in multislice CT. Eur Radiol 15:1888–1897
28. Itoh S, Takada A, Satake H, Ota T, Ishigaki T (2005) Diagnostic value of multislice CT for pancreas divisum: Assessment with oblique coronal reconstruction images. J Comput Assist Tomogr 29:452–460
29. Itoh S, Fukushima H, Takada A, Suzuki K, Satake H, Ishigaki T. CT appearance of anomalous pancreaticobiliary junction: Assessment with high-resolution multiplanar reformatted images in multislice CT. Am J Roentgenol (in press)